Acid Sphingomyelinase-Deficient Mice Mimic the Neurovisceral Form of Human Lysosomal Storage Disease (Niemann–Pick Disease)

Bernd Otterbach and Wilhelm Stoffel
Institute of Biochemistry
Medical Faculty
University of Cologne
D-50931 Cologne
Federal Republic of Germany

Summary

We have generated an acid sphingomyelinase (aS-Mase)-deficient mouse line by gene targeting. This novel strain of mutant mouse mimics the lethal, neurovisceral form of the human sphingomyelin storage disease, known as Niemann–Pick disease. Homozygous mice accumulate sphingomyelin extensively in the reticuloendothelial system of liver, spleen, bone marrow, and lung, and in the brain. Most strikingly, the ganglionic cell layer of Purkinje cells of the cerebellum degenerates completely, leading to severe impairment of neuromotor coordination. The Niemann–Pick mouse might facilitate studies on the function of aSMase in the generation of ceramide as proposed second messenger in the intracellular signaling pathways and across the plasma membrane. Furthermore, it provides a suitable model for the development of strategies for somatic gene therapy.

Introduction

Sphingomyelin is a main lipid constituent of the plasma membrane and of plasma membrane–derived membranes (e.g., endosomes/lysosomes) of mammalian cells. Lysosomal acid hydrolases play an important role in the turnover of membrane lipids of any cell. Among them, acid sphingomyelinase (aSMase, sphingomyelin phosphodiesterase, EC 3.1.4.12) hydrolyzes sphingomyelin to ceramide and phosphocholine. The enzyme is present in endosomes/lysosomes of all cells but particularly in cells of the reticuloendothelial system (RES) of liver (Kupffer cells), spleen, bone marrow, lung, and in macrophages. The autosomal recessive disease known as Niemann–Pick disease (Brady, 1987; Klenk, 1935; Niemann, 1914; Pick, 1927) is characterized by a partial or complete loss of acid sphingomyelinase. Niemann–Pick disease occurs in different phenotypes: the neurovisceral type A (NPA) and the visceral, nonneuropathic form, type B (NPB). The severity of symptoms is greater and the life span shorter in NPA patients than in NPB patients. A third form, Niemann–Pick disease type C, is a lipidosis nosologically totally different from types A and B. It is not primarily caused by a loss of sphingomyelinase activity (Crocker, 1961). Cholesterol is stored in vesicles intracellularly (Vanier et al., 1991).

The recent isolation and characterization of human aSMase and the cloning and sequencing of the cDNA (Quintern et al., 1989) and the coding sequence of the human gene (Newrzella and Stoffel, 1992; Schuchman et al., 1991) revealed that aSMase is a 627 amino acid residue glycoprotein of 64 kDa that is encoded in six exons. The gene is distributed over approximately 5 kb in the asmase locus on chromosome 11p15.1-15.4 (Pereira et al., 1991). Several different mutations, so far mostly point mutations, in the human asmase gene have been found that cause NPA or NPB. The mutations lead either to a complete loss or to a residual aSMase activity (0%–10% of normal activity). The molecular basis of the development of the neurovisceral (type A) and visceral forms (type B) is not understood. Existing animal models are insufficiently characterized on the genetic level (Bundza et al., 1979; Fredrickson et al., 1969; Snyder et al., 1982). They represent mostly type C Niemann–Pick phenotypes.

We recently isolated and characterized the mouse asmase gene (Newrzella and Stoffel, 1992). Sequence comparison indicates that the mouse and human asmase genes are highly similar in size, gene organization, and nucleotide sequence of exons and introns.

Here we report the generation and characterization of an aSMase-deficient mouse line. Mice were generated by gene targeting using homologous recombination in embryonic stem (ES) cells. We have disrupted the wild-type asmase gene in exon III by the insertion of the neomycin (neo) resistance gene.

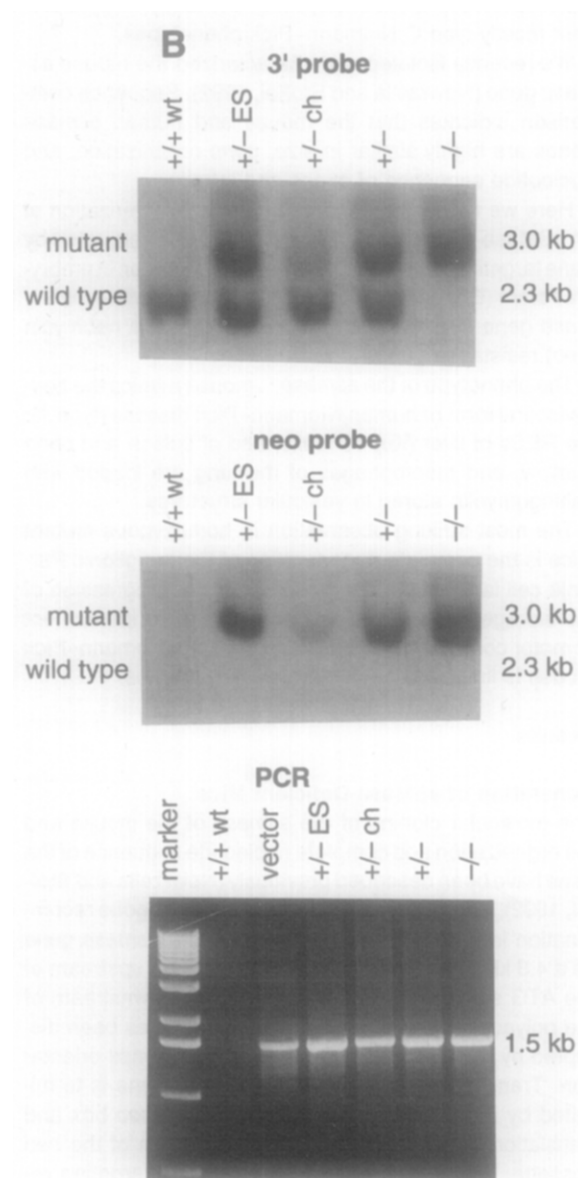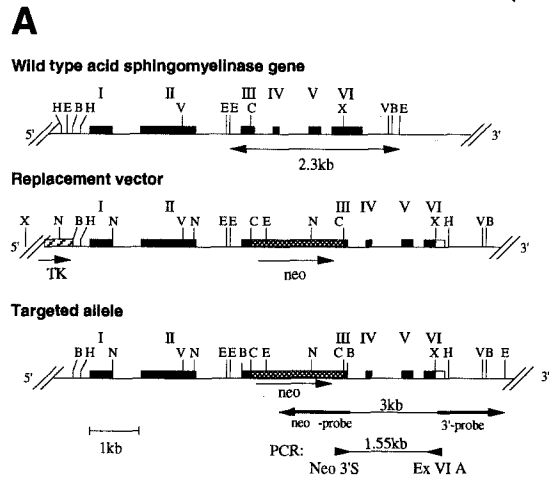The phenotype of the asmase−/− mouse mimics the neurovisceral form of human Niemann–Pick disease (type A): the RESs of liver (Kupffer cells) and of spleen and bone marrow, and macrophages of the lung are loaded with sphingomyelin stored in vesicular structures.

The most striking observation in homozygous mutant mice is the complete degeneration of the ganglionic Purkinje cell layer of the cerebellum with the progression of the storage disease, associated with severe impairment of motor coordination. The life span of the Niemann–Pick mouse is limited to approximately 4–6 months.

Results

Generation of aSMase-Deficient Mice

The molecular cloning of the asmase of the mouse and the organization and complete nucleotide sequence of the gene have been described previously (Newrzella and Stoffel, 1992). The targeting construct for homologous recombination in ES cells harbors the complete asmase gene as a 4.8 kb BamHI fragment, starting 781 bp upstream of the ATG start codon and ending 160 bp downstream of the polyadenylation site. Exon III (174 bp) has been disrupted by the insertion of the neo gene in sense orientation. Transcription of the altered asmase gene is terminated by the polyadenylation signal of the neo box and translation by several stop codons upstream of the neo cassette. Four ES cell clones carrying the targeting replacement construct in the asmase locus were obtained by electroporation. They were transferred into blastocysts of C57BL/6 donors, which were used for the generation

A

Wild type acid sphingomyelinase gene

Replacement vector

Targeted allele

B

3' probe

neo probe

PCR

of male chimeric mice. Cross-breeding of chimeric males with C57BL/6 females yielded heterozygotes, which were intercrossed to obtain homozygous mutant mice. For the analysis of genomic DNA of ES cells and for allelic typing of transgenic mice, tail DNA of chimeric mice and of heterozygous and homozygous offspring was isolated and digested with EcoRI. Southern blot analysis was performed by using the 3' and neo probes indicated in Figure 1A. The expected sizes of fragments hybridizing with the 3' and neo probes are given below the corresponding wild-type (asmase$^{+/+}$) and mutant (asmase$^{-/-}$) alleles. The release of a 3 kb EcoRI fragment indicated the mutant allele and a 2.3 kb fragment the wild-type allele, respectively.

Polymerase chain reaction (PCR) analysis with the 5' and 3' primers (Figure 1A) was carried out to confirm the homologous recombination event further. The 1.55 kb PCR fragment expected from use of the 5' and 3' primers (Figure 1B) was obtained only with the mutant allele as template.

Development of aSMase-Deficient Mice

The asmase mutant mice developed indistinguishably from the wild type for a period of 8–10 weeks. At this point, the homozygous mutant mice developed a fine tremor of the whole body and a severe intention tremor, and their gait became increasingly ataxic: tottering with zigzag movement, characteristic of cerebellar dysfunction.

Figure 1. Generation of aSMase-Deficient Mice

(A) Schematic presentation of the wild-type asmase mouse gene, the asmase replacement vector, and the mutant targeted allele. The targeting construct for homologous recombination in ES cells harbors the complete asmase gene as a 4.8 kb BamHI fragment, starting 781 bp upstream of the ATG start codon and ending 160 bp downstream of the polyadenylation site (Newrzella and Stoffel, 1992). Closed boxes indicate exons I–VI, the solid line extragenic sequences of the asmase. The neo cassette driven by the tk promoter (stippled box) was inserted into the BclI site of exon III, the thymidine kinase gene (tk) 5' to the asmase gene for negative selection (open box). For the detection of homologous recombinants, genomic DNA of ES clones and tail DNA of chimeric mice was isolated and digested with EcoRI. The expected sizes of fragments hybridizing with the 3' and neo probe are indicated below the corresponding wild-type and mutant asmase loci. Restriction enzymes: B, BamHI; C, BclI; E, EcoRI; V, EcoRV; H, HindIII; X, XbaI. (B) Southern blot hybridization analysis of tail DNA of ES cell clones (+/− ES), wild-type mice (+/+ wt), chimeric mice (+/− ch), heterozygous mice (+/−), and homozygous (−/−) mice. Tail DNA was digested with EcoRI, size-fractionated by agarose gel electrophoresis (0.8%), blotted to gene screen filter, and hybridized with the 1.3 kb 3' fragment of the asmase DNA (top) and the neo probe (center), as indicated in (A). Wild-type mice (+/+ wt), ES cells (+/− ES), chimeric mice (+/− ch), heterozygous mice (+/−), and homozygous mice (−/−). Bottom, PCR analysis. Positions of the primers used for the PCR are indicated in (A). The 3' oligodesoxyinucleotide primer hybridizes outside of the 3' end (XhoI insertion site) of the replacement targeting construct; the 5' primer (neo 3') is positioned in the neo gene. The 1.55 kb PCR fragment indicates the presence of the neo cassette in the 3 kb EcoRI fragment in homologous recombined hetero- (+/−) and homozygous (−/−) mice. The order of the lanes is the same as that given for the Southern blot analysis (upper two panels). Vector: DNA contains the complete replacement asmase knockout construct out of which the XhoI fragment was isolated and used for electroporation of ES cells.
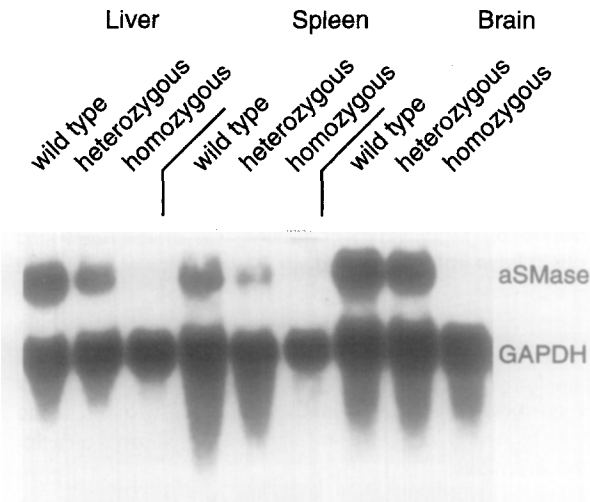
Liver Spleen Brain

Figure 2. *asmase* mRNA Is Absent in the Total RNA of Liver, Spleen, Brain, and Lung of Homozygous *asmase*⁻/⁻ Mice

Northern blot hybridization analysis of liver, spleen, and brain RNA. Total RNA of wild-type (C57BL/6) mice and hetero- and homozygous mutant mice was separated by formaldehyde–agarose (1.2%) gel electrophoresis, transferred to a gene screen membrane, hybridized with a randomly labeled full-length *asmase* cDNA, and compared with those of the intrinsic GAPDH, which was probed with a GAPDH-specific cDNA fragment as a control. The intensities of the hybridization signals were quantified by use of a Phosphorimager (Molecular Dynamics).

Hepatosplenomegaly becomes visible around day 60 after birth. In the final stage, around day 120 after birth, the mutant mice become severely dyspneic. This pulmonary distress leads to severely restricted physical activity and finally to death. The life expectancy of aSMase-deficient mice is around 4 months.

Characterization of *asmase* Deficiency in Mutant Mice

asmase mRNA Is Absent in All Organs

The *neo* resistance gene introduced into exon III of the *asmase* gene disrupts the coding region at amino acid 370. Northern blot analysis of total RNA of liver, spleen, and brain of homozygous *asmase*⁻/⁻ mice revealed no *asmase*-specific transcripts, neither truncated nor full length, when a full-length *asmase* cDNA fragment was used as probe (Figure 2). A faint high molecular transcript hybridizes with the cDNA and *neo* probes. Hybridization with a *neo* probe indicated that the size of this transcript is approximately 3.6 kb, which is the size of a readthrough transcript (*asmase* mRNA plus *neo* gene). The 2.4 kb *asmase* mRNA of heterozygous mutants was reduced to approximately one half, as estimated from the intensities of the hybridization signals, which were quantified by a Phosphorimager (Molecular Dynamics) and compared with those of the intrinsic glyceraldehyde 3-phosphate dehydrogenase (GAPDH) monitored by a specific cDNA probe as a control. The structure of the 3.6 kb transcript was also verified by reverse transcription–PCR using appropriate

A

	geno-type	protein (μg)	dpm	% activity	spec. act.
liver	+/+	3; 5	3410; 6035	100; 100	100
	+/-		2395; 1535	70; 42	
	-/-		0; 0	0; 0	
spleen	+/+	3; 5	1535; 5235	100; 100	80
	+/-		1395; 2120	55; 40	
	-/-		0; 0	0; 0	
brain	+/+	3; 5	6525; 14215	100; 100	210
	+/-		3850; 9720	59; 68	
	-/-		0; 0	0; 0	

B

	geno-type	protein (μg)	aSmase dpm	nSmase dpm
liver	+/+	25	8743; 8464	2728; 1931
	-/-		0; 0	317; 371
spleen	+/+	25	3322; 3860	897; 741
	-/-		0; 0	261; 309
brain	+/+	25	10076; 10922	27762; 29646
	-/-		0; 0	20101; 26602

Figure 3. Homozygous Mice Show a Complete Lack of aSMase but Not of nSMase

Enzyme assays of aSMase and nSMase of wild-type and *asmase*⁻/⁻ mice are recorded as dpm, released from [methyl-¹⁴C]sphingomyelin during the 1 hr incubation at 37°C.

(A) The 18,000 × g supernatant of homogenized and detergent-lysed specimen of liver, spleen, and brain tissue were assayed for aSMase activity by incubating the respective cell extract with the labeled [methyl-¹⁴C]sphingomyelin substrate. The water-soluble radioactivity released during the reaction was measured.

(B) The residual neutral sphingomyelinase (nSMase) in liver, spleen, lung, and brain was assayed at neutral pH (pH 7.4), with the homogenate (600 × g) of the respective tissues containing the nSMase resident in the plasma membrane. Aliquots (10 μg and 25 μg) of the homogenates of the respective tissues were used as enzyme sources.

primers of *asmase* exon III and the *neo* box (data not shown).

Homozygous *asmase* Mutant Mice Completely Lack aSMase but not Neutral Sphingomyelinase Activity

aSMase and the residual neutral sphingomyelinase (nSMase) were assayed in total protein extract of liver, spleen, and brain of wild-type mice and hetero- and homozygous mutants. The release of the [methyl-¹⁴C]phosphorylcholine group from [methyl-¹⁴C]sphingomyelin into the aqueous phase was measured. No aSMase activity was measurable in the homozygous mutants, and a reduction to approximately one half was found in the heterozygous mutants (Figure 3).

Residual nSMase in liver, spleen, lung, and brain was assayed under neutral reaction conditions (pH 7.4). The homogenate of the respective tissues containing the nSMase resident in the plasma membrane (600 × g supernatant) was assayed for sphingomyelinase activity. The analyses of aSMase with the homogenates as enzyme source match those obtained with the 18,000 × g supernatant of liver, spleen, and brain of wild-type, *asmase*⁺/⁻, and *asmase*⁻/⁻ mice. Under the assay conditions for nSMase,
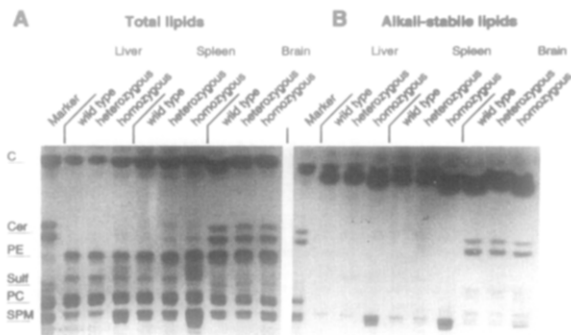
Figure 4. Total Lipid Extracts of Liver, Spleen, and Brain Show Massive Accumulation of Sphingomyelin

(A) Total lipid extracts of liver, spleen, and brain of wild-type mice and hetero- and homozygous mutant mice were separated by TLC.
(B) Ester lipids were saponified and the alkali-stabile lipids separated in the same solvent system (chloroform–methanol–water, 65:25:4). Bands were visualized with a sulphuric acid spray. Phospholipids among the total and alkali-stabile lipids were also stained with Zinzadze reagent (Dittmer and Lester, 1964). Abbreviations: C, cholesterol; cer, cerebroside; PE, phosphatidylethanolamine; sulf, sulfatide; PC, phosphatidylcholine; SPM, sphingomyelin.

25%–30% of the aSMase activity of the respective tissue is still measurable at pH 7.4. This has been demonstrated with purified human aSMase (unpublished data). Therefore, the numbers in Figure 3 for nSMase activity of $asmase^{+/-}$ and $asmase^{-/-}$ mice must be corrected by this contribution of aSMase. The SMase activity in $asmase^{-/-}$ liver, spleen, and brain reflects the actual nSMase activity in the respective tissues. Thus, nSMase activity is apparently not altered by the loss of aSMase expression.

Interestingly, Figure 3 indicates that nSMase activity in brain of wild-type mice is three times higher than aSMase activity. nSMase in homozygous $asmase^{-/-}$ mice is only slightly reduced as compared with its levels in parenchymous tissues rich in RES such as spleen, liver, and lung.

Lipid Analysis of Wild-Type Mice and Hetero- and Homozygous Mutant Mice

Sphingomyelinase-deficient mice accumulate large amounts of sphingomyelin in RES cells. We limited the analysis of total lipids to the liver, spleen, and brain, which are of central interest in NPA and NPB. Total lipids were extracted with chloroform–methanol from liver, spleen, and brain specimens of wild-type mice and hetero- and homozygous mutant mice. Aliquots of the total lipid extracts were saponified. Esterlipids were hydrolyzed to water-soluble potassium salts of fatty acids and the polar head group components (glycerol, phosphate, and the respective bases). Sphingomyelin and the other sphingolipids are alkali resistant and therefore dissolve together with cholesterol in the chloroform phase. Figure 4 presents the thin-layer chromatograms (TLC) of total and alkali-stabile lipids of the liver, spleen, and brain of wild-type mice and hetero- and homozygous mutant mice. Components of total lipid extracts (Figure 4A) and unsaponifiable lipids (sphingomyelin, cerebrosides, sulfatides, gangliosides, and cholesterol; Figure 4B) were visualized with sulphuric acid. Phospholipids present in the total lipid ex-

tract and among the unsaponifiable lipid components were visualized with Zinzadze reagent (data not shown).

The most prominent lipid in the liver and spleen of homozygous mutant mice is sphingomyelin. The accumulation of sphingomyelin is also visible in the lipid extract of brains, although it is by far not as pronounced as in the RES of liver and spleen. Sphingomyelins separate in TLC into two bands, sphingomyelins containing the unsaturated long chain base sphingosine (lower Rf value; lower band) and those with dihydrosphingosine (higher Rf value; upper band). They are both substituted with fatty acids of chain lengths C_{16} to C_{24}. Cerebrosides and sulfatides also split into bands, however, owing to their acyl groups. The bands with lower Rf values are the α-hydroxy fatty acids, those with higher Rf values the n-fatty acid–substituted galactosylceramides.

Homozygous asmase⁻/⁻ Mice Show Severe Hepatosplenomegaly

Inspection of the parenchymous organs of the opened abdomen of wild-type mice and hetero- and homozygous aSMase-deficient mice revealed an enlarged liver and spleen in the homozygous mice. The wet weight of the total liver of homozygous $asmase^{-/-}$ mice had increased about 1.5 times, and that of the spleen varied but often reached twice the weight of age- and sex-matched wild-type mice in the final stage. The sacrificed mice were immediately perfused with 4% paraformaldehyde in phosphate-buffered saline (PBS), and liver, spleen, lung, and brain were excised and postfixed for paraffin or cryo- and ultrathin sections for electron microscopy.

In histology, Kupffer cells of liver and hepatocytes are swollen and have a foam cell appearance, with extended vacuolation throughout the whole cytoplasm. The nucleus of RES cells appears to be dislocated by the globular or vesicular structures to the periphery. Figure 5a presents the histology of a liver acinus of a wild-type (upper left) and a homozygous $asmase^{-/-}$ mutant mouse (right). Arrows point to Kupffer cells loaded with sphingomyelin (foam cells). In electron microscopy, the Kupffer cell, given here as a representative example of the foam cell morphology of the macrophage RES of the asmase-null mutant, reveals that lysosomes are filled with stacked membranes of stored sphingomyelin, forming myelin figures (Figure 5B). The red pulp of spleen is filled with large, only faintly stained foam cells (Figure 5, center). Numerous megakaryocytes scattered through the red and white pulp can be seen at lower magnification.

Alveoli of the lungs of homozygous mice are clotted with nodular, diffuse reticulate infiltrations that consist of lipid-loaded histiocytes. Alveoli of the lungs of wild-type mice (Figure 5, left) are compared with those of mutant mice lacking aSMase (right).

Ganglion cells of homozygous mice in gray matter of the central nervous system (CNS) are frequently swollen with pale vacuolation in cytoplasm. The cortical structure appears slightly disrupted, owing to the loss of cells in the cerebral and cerebellar cortex. A slight gliosis is seen in gray and white matter.

The endothelium of the plexus chorioideus is swollen and heavily loaded with foam cells. Homogeneously
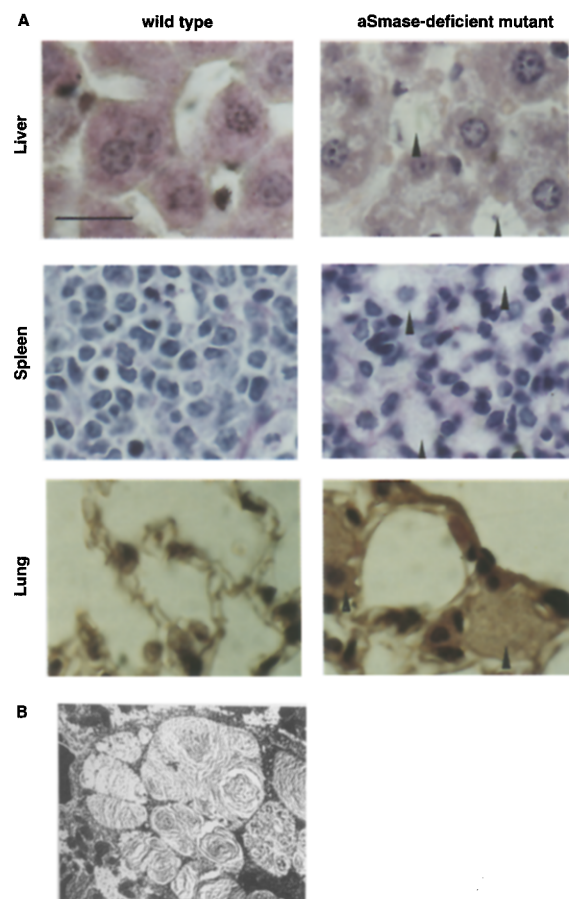
Figure 5. Cells of the RES Macrophage System of Liver, Spleen, and Lung Are Transformed to Lipid-Loaded Foam Cells

(A) Liver from wild-type mice (left) and from homozygous aSMase-deficient mice (right). Arrows mark some of the RES foam cells (enlarged Kupffer cells), the nuclei of which are dislocated to the periphery by sphingomyelin-loaded lysosomes. The spleen of the wild-type mouse (left) shows a regular pulp. In homozygous mutants (right), the red pulp is disrupted by interspersed foam cells and many megakaryocytes. Lung alveoli of homozygous mutant mouse (right) are clotted with histiocytes that are degenerated to large lipid-loaded foam cells. Left, wild-type mouse. Sections (3–5 μm) of liver and lung were stained with hematoxylin–eosin; sections of spleen were stained with PAS. Scale bar, 80 μm.
(B) Electron microscopy of Kupffer cell in the liver of $asmase^{-/-}$ mice. The cell is filled with lysosomes packed with stacked membraneous, myelin-like structures consisting of stored sphingomyelin.

stained, isolated large cells are loosely deposited within the spinal fluid space of the plexus.

The most striking observation is the progressive and finally complete degeneration of the Purkinje cell stratum (Figure 6), which occurs within 60–90 days after birth in homozygous mice. Few residual Purkinje cells are persistent; these are packed with lipid-loaded lysosomes. They have lost their flask-shaped form, and their nuclei are in the process of lysis. At earlier stages, more Purkinje cells with the foam cell morphology are seen, indicating the progression of the storage disease with age predominantly, if not selectively, in this cell layer. The loss of the Purkinje cell layer explains the severe impairment of motor coordination described below and known as cerebellar ataxy.
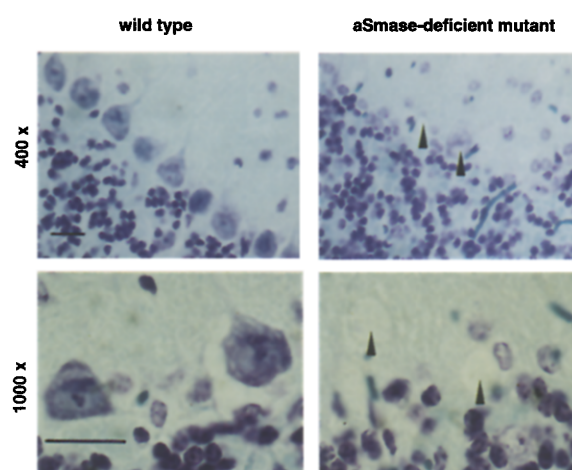
Figure 6. Purkinje Cells of Homozygous Mutant aSMase-Deficient Mice Degenerate Selectively and Completely

Section of cerebellum of control wild-type mice (left). Flask-shaped Purkinje cells line up as a single ganglionic stratum in the deepest part of the molecular layer adjacent to the granular cell layer of cerebellum. In the homozygous mouse (right), only a few residual degenerated Purkinje cells are visible. The bordering granular layer appears irregular; granular cells have normal appearance. Sections (3–5 μm) of cerebellum were stained with luxol–cresyl violet. Scale bar, 80 μm.

Cerebellar Motor Coordination Is Lost in asmase Mutant Mice

Cerebellar ataxy is the dominant neuropathological symptom. Locomotor ataxy is evidenced by the ataxic gait and the intention tremor. We documented the cerebellar ataxic gait by the hind foot pattern (Aiba et al., 1994) of wild-type and of two aSMase-deficient mutant mice at age 90 days after birth (Figure 7). The gait is straddle-legged. Lines at the bottom of Figure 7 mark the average distance between the print of the left and the right hind foot. The pattern also visualizes the contact of the foot sole with widespread toes and the plantar part of hind feet. The steps are shorter, as indicated by the average distance between foot prints.

We used the rotarod test for testing the motor coordination. Cerebellar motor coordination decayed along with the loss of Purkinje cells. At postnatal day 50, the motor deficit of mutant mice became apparent. Mutant mice 3–4 months old were unable to stay on the resting or extremely slowly rotating rod (Figure 8).

Discussion

The molecular basis of Niemann–Pick disease with the massive storage of sphingomyelin in the lysosomes of RES cells is confined to alterations of the asmase gene. This results in a change of the primary structure and reduced catalytic activity of aSMase. Following the isolation of asmase and the cloning of asmase-specific cDNA, several point mutations have been defined in asmase of fibroblasts isolated and cultured from Niemann–Pick disease patients. In most cases, the level of aSMase activity is greatly reduced. The wide range of phenotypes of late onset neurovisceral sphingomyelinosis variants with residual activity of a mutant asmase may be reconciled on
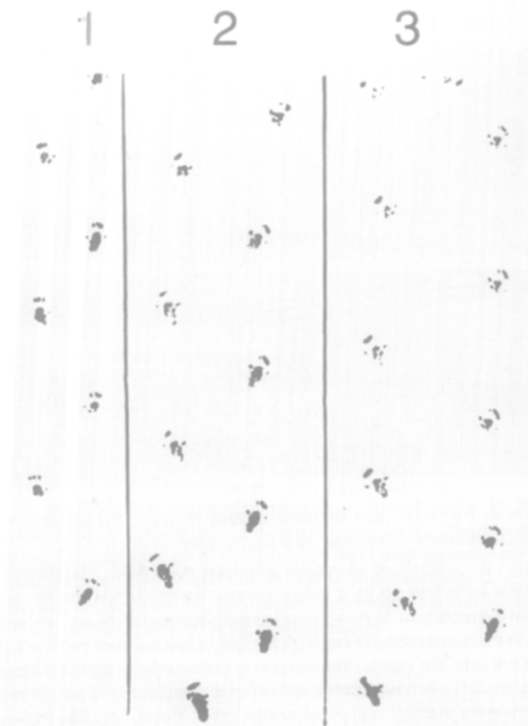
Figure 7. Gait Pattern of Wild-Type and asmase⁻/⁻ Mice

Hind foot pattern of wild-type (lane 1) and homozygous 90-day-old mutant mice (lanes 2 and 3). Mutant mice walk in short steps with a wide base between their hind feet. Bars under the foot pattern refer to the narrow traces of wild-type hind footprints and those of two mutant mice of the same age. Footprints also indicate a broad stabilizing plantar contact with widespread toes. A straightforward movement of the mutant mice is only possible between narrow barriers lining the pathway.

Figure 8. Rotarod Test Shows Impaired Motor Coordination

Motor coordination declines with age in parallel with the degeneration of the Purkinje cell layer. Whereas wild-type mice (n = 6) remain on the rotating rod for the times indicated, the mutant mice beyond postnatal day 50 fell from the rod rotating at 8 rpm immediately. At the age of 4 months, they were no longer able to stay on the rod rotating at 0.4 rpm; some were not even able to stay on the resting rod.

the basis of a kinetic model that correlates the residual activity with the rate of degradation of sphingomyelin in the lysosome (Conzelmann and Sandhoff, 1991). The variant phenotype of Niemann–Pick disease has also been taken as an argument for the presence of aSMase isoenzymes (Callahan and Khalil, 1976).

However, neither the numerous point mutations in the asmase gene nor the few genetically uncharacterized animal models have so far allowed an unambiguous definition of the asmase⁻/⁻ phenotype.

asmase⁻/⁻ Mice Develop Severe Sphingomyelin Storage Disease

We generated a mouse model with a complete lack of the lysosomal (acid) sphingomyelinase (Niemann–Pick mouse) to study the molecular and cellular basis of the complete loss of aSMase, particularly with respect to the involvement of the CNS.

The targeting construct introduced into ES cells by homologous recombination replaced the asmase gene. The resulting asmase-null mutant showed a complete absence of asmase mRNA in Northern blot hybridization analysis in all tissues studied. Consequently, all tissues of the homozygous mutant mice are completely devoid of aSMase

activity. Owing to the lack of the enzyme, the homozygous mutant mouse develops a severe sphingomyelin storage in the lysosomes of the RES macrophage system, which appear morphologically as large subcellular vesicular structures. They are filled with stacked membrane-like structures (myelin figures), as seen through the electron microscope, similar to those described previously in the liver of Niemann–Pick patients (Brady, 1987) (Figure 5B). Sphingomyelin storage is generalized in the RES cells, particularly in visceral organs, here documented for liver, spleen, and lung (Figure 5A).

The massive storage of sphingomyelin in histiocytes (foam cells) in the lung leads to diffuse reticular and nodular infiltrations with obstruction of the alveoli, which causes severe pulmonary incapacitance.

Complete Degeneration of Purkinje Cell Stratum in asmase⁻/⁻ Mice

Besides the widely distributed storage of sphingomyelin in neuronal and glial cells, the most striking observation in CNS morphology of the aSMase-deficient homozygous mouse is the complete degeneration of the Purkinje cell stratum in the cerebellum. The degeneration of Purkinje cells is a rapidly progressing process, the first signs being observed during postnatal week 10. It explains the ataxic gait and intention tremor. The rapid deterioration of motor coordination with age is documented in the rotarod test. The asmase⁻/⁻ mice fail with increasing age to stay on the slowly rotating or resting rod.

Perspectives

The question remains why Purkinje cells selectively and not all neurons and glia cells manifest massive sphingomyelin storage with subsequent cell death. Is it the enhanced membrane turnover of Purkinje cells? Their neuronal activity exceeds by far that of most other cell types of the CNS, owing to their prominent role in motor plasticity (Konnerth et al., 1990). Purkinje cells of the cerebellar cortex form excitatory and inhibitory synapses with parallel and climbing fibers on the excitatory side and from basket cells

(pH 7.2), 0.1% NP-40, and 5 U of Trasylol (Bayer) in a Waring blender. The homogenate was stirred for 1 hr at 4°C and centrifuged at 18,000 × g for 45 min. The supernatant was used for the enzyme assay.

Protein was determined with the bicinchoninic acid (BCA) protein assay reagent, according to the instructions of the manufacturer (Pierce, Rockford, IL). [Methyl-^{14}C]sphingomyelin (Stoffel et al., 1971) (8000 dpm/nmol) was dissolved at a concentration of 1 nmol/μl in 0.1 M sodium acetate (pH 4.5), 0.1% NP-40. The substrate solution (10 μl) was incubated with 10 μl and 20 μl of enzyme solution, respectively, and diluted to 200 μl with the above buffer and incubated for 1 hr at 37°C. To this, 100 μl of 0.1% phosphocholine was added. For nSMase, the homogenate (600 × g) of liver, spleen, and brain of wild-type mice and homozygous mutant mice was used as enzyme source. The assay was carried out under the same conditions as described for aSMase, but substituting the pH 4.5 acetate buffer by a 0.1 M Tris–HCl (pH 7.4), 2 mM MgCl$_2$, 0.1% NP-40 buffer. Ceramide and excess substrate were extracted with 800 μl of chloroform–methanol (2:1 v/v). Aliquots (100 μl) of the aqueous phase were counted in 10 ml of Bray solution in a scintillation counter.

Lipid Analysis
Total Lipid Extracts
Specimens of liver, spleen, and brain of wild-type mice and hetero- and homozygous aSMase-deficient mice were homogenized in 10 vol of chloroform–methanol (2:1 v/v) with an ultraturrax. The homogenate was centrifuged at 600 × g, the clear supernatant collected, and the extraction repeated. The combined supernatant was evaporated to dryness on a rotary still. Lipids were dissolved in equal volumes of chloroform–methanol (2:1).

Alkaline Hydrolysis of Lipids
Aliquots of the total lipid extract were saponified in 1 ml of 0.5 N methanolic KOH at 37°C for 4–6 hr. Water (0.5 ml) was added and the mixture extracted three times with chloroform. Phases were separated by centrifugation. The combined chloroform extracts were concentrated to dryness. Aliquots of total and alkali-stabile lipids were streaked on coated high performance TLC plates for separation with the solvent system chloroform–methanol–water, 65:25:4. Phospholipid bands were visualized by spraying the plate with Zinzadze reagent (Dittmer and Lester, 1964). For fatty acid analysis, the two sphingomyelin bands (Figure 4) were scraped from the plates, separately transferred into small Sovirel tubes, and transesterified with 5% (w/w) methanolic HCl (1 ml) at 80°C for 4 hr under nitrogen. Water (1 ml) was added, and fatty acid methylesters were extracted twice with 1 ml of hexane. The solvent was evaporated in a stream of nitrogen. The fatty acid methylesters were dissolved in chloroform for gas chromatography: a capillary column (15 m), coated with DB-225 (J and W Scientific), was used in a model 8000 GLC apparatus Erba, with helium as carrier gas. A temperature program (5°C/min) between 180°C and 200°C was run.

Histology
Wild-type mice and hetero- and homozygous aSMase-deficient mice of different ages were sacrificed in a CO$_2$ atmosphere. Upon inspection of the opened abdomen, liver and spleen of the homozygous mice appeared enlarged and slightly yellowish. Mice were immediately perfused with 20 ml of 2.5% paraformaldehyde in PBS through the left ventricle of the heart with the right atrium opened. Liver, spleen, lung, intestine, and brain were excised and postfixed for an additional 12 hr in the same fixative. They were paraffin embedded, following standard procedures. Microtome sections (3–6 μm) were mounted on polylysine-coated slides and stained with hematoxylin–eosin, cresyl violet, periodic acid–Schiff reagent (PAS), or luxol–cresyl violet as indicated in the legends to figures.

Neuromotor Activity Tests
The rotarod test was carried out with a rotarod apparatus manufactured in the local machine shop. It consisted of a plastic rod (3 cm diameter) with a gritted surface. Compartments of 10 cm on the rod were separated by discs 30 cm in diameter. The rod was rotated by a step motor at speeds of 0.4, 0.8, 1.6, 4.0, and 8.0 rpm. Groups of age-, size-, and sex-matched wild-type and mutant mice were studied. They were placed on the rod in separated compartments, and the time each

mouse remained on the rod at defined speeds of rotation was measured. Times of repeated experiments were averaged.

Footprint analyses were carried out as described (Aiba et al., 1994).

References

Aiba, A., Kano, M., Chen, C., Stanton, M. E., Fox, G. D., Herrup, K., Zwingman, T. A., and Tonegawa, S. (1994). Deficient cerebellar long-term depression and impaired motor learning in mGluR1 mutant mice. Cell 79, 377–388.

Bradley, A. (1987). Production and analysis of chimeric mice. In Teratocarcinomas and Embryonic Stem Cells: A Practical Approach, E. J. Robertson, ed. (Oxford: IRL Press), pp. 113–151.

Brady, R. (1987). Sphingomyelin lipidosis: Niemann–Pick disease. In The Metabolic Basis of Inherited Disease, J. B. Stanbury, J. B. Wyngaarden, D. S. Fredrickson, J. L. Goldstein, and M. S. Brown, eds. (New York: McGraw–Hill Book Company), pp. 831–841.

Bundza, A., Lowden, J. A., and Charlton, K. M. (1979). Niemann–Pick disease in a poodle dog. Vet. Pathol. 16, 530–538.

Callahan, J. W., and Khalil, M. (1976). Sphingomyelinase and the genetic defects in Niemann–Pick disease. In Current Trends in Sphingolipidoses and Allied Disorders, B. W. Volk and L. Schneck, eds. (New York: Plenum Press), pp. 367.

Chatterjee, S. (1993). Neutral sphingomyelinase. Adv. Lipid Res. 26, 25–48.

Chomczynski, P., and Sacchi, N. (1987). Single-step method of RNA isolation by acid guanidinium thiocyanate–phenol–chloroform extraction. Anal. Biochem. 162, 156–159.

Conzelmann, E., and Sandhoff, K. (1991). Biochemical basis of late onset neurolipidoses. Dev. Neurosci. 13, 197–204.

Crocker, A. C. (1961). The cerebral defect in Tay–Sachs and Niemann–Pick disease. J. Neurochem. 7, 69.

Dittmer, J., and Lester, R. (1964). A simple, specific spray for the detection of phospholipids on thin-layer chromatograms. J. Lipid Res. 5, 126–127.

Divecha, N., and Irvine, R. F. (1995). Phospholipid signaling. Cell 80, 269–278.

Fredrickson, D. S., Sloan, H. R., and Hansen, C. T. (1969). Lipid abnormalities in foam cell reticulosis of mice, an analogue of human sphingomyelin lipidosis. J. Lipid Res. 10, 288–293.

Jarvis, W. D., Kolesnick, R. N., Fornari, F. A., Taylor, R. S., Gerwitz, D. A., and Grant, S. (1994). Induction of apoptotic DNA damage and cell death by activation of the sphingomyelinase pathway. Proc. Natl. Acad. Sci. USA 91, 73–77.

Klenk, E. (1935). Über die Natur der Phosphatide und anderer Lipide des Gehirns und der Leber bei der Niemann–Pick-Krankheit. Hoppe-Seyler's Z. Physiol. Chem. 235, 24–36.

Konnerth, A., Llano, I., and Armstrong, C. M. (1990). Synaptic currents in cerebellar Purkinje cells. Proc. Natl. Acad. Sci. USA 87, 2662–2665.

Laird, P. W., Zijderveld, A., Linders, K., Rudnicki, M. A., Jaenisch, R., and Berns, A. (1991). Simplified mammalian DNA isolation procedure. Nucl. Acids Res. 19, 4293.

Machleidt, T., Wiegmann, K., Henkel, T., Schütze, S., Baeuerle, P., and Krönke, M. (1994). Sphingomyelinase activates proteolytic NF-κB-α degradation in a cell-free system. J. Biol. Chem. 269, 13760–13765.

Mathias, S., Dressler, K. A., and Kolesnick, R. N. (1991). Characterization of a ceramide-activated protein kinase: stimulation by tumor necrosis factor alpha. Proc. Natl. Acad. Sci. USA 88, 10009–10013.

Newrzella, D., and Stoffel, W. (1992). Molecular cloning of the acid sphingomyelinase of the mouse and the organization and complete nucleotide sequence of the gene. Hoppe-Seyler's Z. Biol. Chem. 373, 1233–1238.

Niemann, A. (1914). Ein unbekanntes Krankheitsbild. Jahrb. Kinderheilkd. 79, 1–10.

Obeid, L. M., Linardic, C., Karolak, L. A., and Hannun, Y. A. (1993). Programmed cell death induced by ceramide. Science 259, 1769–1771.

Pereira, L., Desnick, R. J., Adler, D. A., Disteche, C. M., and Schuchman, E. H. (1991). Regional assignment of the human acid sphingomyelinase gene (SMPD1) by PCR analysis of somatic cell hybrids and in situ hybridization to 11p15.1-p15.4. Genomics 9, 229–234.

Pick, L. (1927). Über die lipoidzellige Splenohepatomegalie Typus Niemann–Pick als Stoffwechselerkrankung. Med. Klinik 23, 1483–1488.

Quintern, L., Schuchman, E., Levran, O., Suchi, M., Ferlinz, K., Reinke, H., Sandhoff, K., and Desnick, R. (1989). Isolation of cDNA clones encoding human acid sphingomyelinase: occurrence of alternatively processed transcripts. EMBO J. 8, 2469–2473.

Raines, M. A., Kolesnick, R. N., and Golde, D. W. (1993). Sphingomyelinase and ceramide activate mitogen-activated protein kinase in myeloid HL-60 cells. J. Biol. Chem. 268, 14572–14575.

Ramirez-Solis, R., Davis, A. C., and Bradley, A. (1993). Gene targeting in embryonic stem cells. Meth. Enzymol. 225, 855–878.

Schuchman, E. H., Suchi, M., Takahashi, T., Sandhoff, K., and Desnick, R. J. (1991). Human acid sphingomyelinase. Isolation, nucleotide sequence, and expression of the full-length and alternatively spliced cDNAs. J. Biol. Chem. 266, 8531–8539.

Snyder, S. P., Kingston, R. S., and Wenger, D. A. (1982). Niemann–Pick disease: sphingomyelinosis of Siamese cats. Am. J. Pathol. 108, 252–254.

Spence, M. W. (1993). Sphingomyelinases. Adv. Lipid Res. 26, 3–23.

Stoffel, W., LeKim, D., and Tschung, T. S. (1971). A simple chemical method for labelling phosphatidylcholine and sphingomyelin in the choline moiety. Hoppe-Seyler's Z. Physiol. Chem. 352, 1058–1064.

Vanier, M. T., Rodriguez-Lafrasse, C., Rousson, R., Duthel, S., Harzer, K., Pentchev, P. G., Revol, A., and Louisot, P. (1991). Type C Niemann–Pick disease: biochemical aspects and phenotypic heterogeneity. Dev. Neurosci. 13, 307–314.

Wiegmann, K., Schütze, S., Machleidt, T., Witte, D., and Krönke, M. (1994). Functional dichotomy of neutral and acid sphingomyelinases in tumor necrosis factor signaling. Cell 78, 1005–1015.